JOURNAL OF COMPUTATIONAL PHYSICS **11**, 333–347 (1973)

The Calculation of Potential Gradients in a Moving Normal Region within a Superconducting Thin Film

DEREK C. BARKER

Department of Electrical Engineering and Electronics,
University of Manchester Institute of Science and Technology, Manchester, England

Received March 13, 1972

A possible realization of Crane's "Neuristor" active transmission line uses a superconducting thin film superimposed on a normally conducting thin film or substrate. Its performance is dependent on velocity-induced asymmetries of the temperature distribution in a small moving normal region within the superconducting film.

The temperature distribution is a function of local Joule heat generation in the normal region (and adjacent conductor). It is, therefore, necessary to obtain information on the current density (or potential gradient) distribution in this area.

In this paper the author discusses the numerical solution to the potential gradient problem. Conditions for convergence of the iterative program for E_x are derived and tested. Computation errors are estimated for E_x and for the continuity equation solution for E_y. Typical results are presented for two values of displacement velocity, using a 37×37 node mesh.

1. INTRODUCTION

The work of Crane [1–3] and others [4–11] on the theory of the "Neuristor" line has led various workers [12–14] to consider physical realizations for this type of active transmission line. Chambers [13] and Green [23] make use of the fact that the transition of a superconductor from its superconducting to its normal phase, under the influence of a current through it, can be influenced by the I^2R heat generated in nearby normal regions. It is possible to control the dimensions of a normal region in this manner, using a sustaining current substantially smaller than the critical current [15]. As the expected thermal relaxation times are of the order of 10^{-8} sec or less, very fast boundary motion is possible.

Chambers proposed a line consisting of two long thin metallic films in intimate contact, one a superconductor, the other a good conductor. A biasing current would flow longitudinally in the superconductor. If a normal region is established (in some unspecified manner), the current would, after entering the normal region, redistribute so as to flow in both films (Fig. 1).

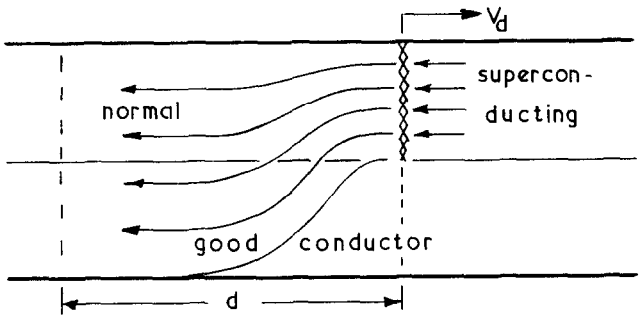

FIG. 1. Current redistribution in normal phase and adjacent conductor.

As a result, the $J^2\rho$ losses, per unit volume, would be greater close to the interphase boundary than at some greater distance into the normal phase. Thus, he anticipated that it would be possible to adjust the biasing current so that the heat generated close to the boundary would be sufficient to cause the boundary to advance into the superconducting phase, while at some distance d into the normal phase it would be insufficient to prevent the restoration of superconductivity. The resultant effect would be a normal region moving along the superconducting line (Fig. 2), and it is easy to show that it would possess the defining characteristics of Crane's hypothetical "Neuristor."

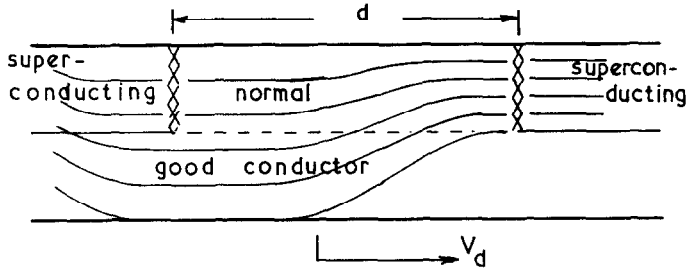

FIG. 2. Initial visualization of current flow patterns in moving normal region and adjacent conductor.

2. STATEMENT OF THE PROBLEM

Chamber's visualization of his proposed line is imperfect in the basic understanding of the current distribution patterns in the normal phase and adjacent good conductor. It has been shown [16] that the electrical relaxation times in both the normal phase and the superconducting phase are such that his anticipated current distribution is obtainable only at velocities in excess of 10^5 m/sec for

1000 Å films. These velocities are clearly excessive for experimental work and it is necessary to consider the current distribution at lower velocities. For zero and very low velocities the current distribution would be symmetrical ($\nabla^2 J = 0$), as shown in Fig. 3. Clearly, the temperature distribution will also be symmetrical, and both boundaries will move outwards or inwards in unison.

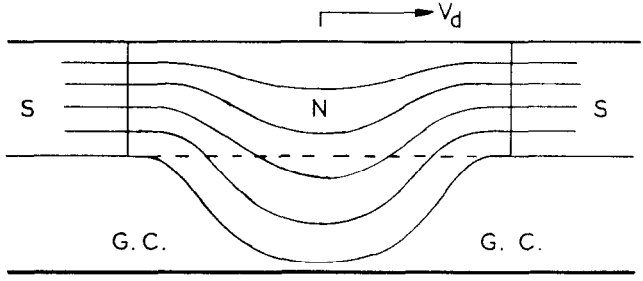

FIG. 3. Current flow patterns in moving normal phase and adjacent conductor for zero and low displacement velocities.

As the velocity is increased, a degree of asymmetry is introduced (Fig. 4) and the heats generated near the boundaries begin to differ, so that it is in principle possible to establish conditions suitable for unidirectional motion of the normal phase. Further examination of the feasibility of this line requires detailed information on the temperature distribution as a function of materials, velocity of propagation and bath temperature.

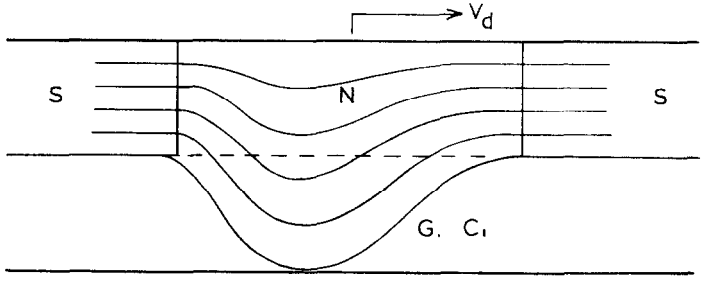

FIG. 4. Current flow patterns in moving normal phase and adjacent conductors, showing anticipated asymmetries due to intermediate displacement velocities.

It is the purpose of this paper to derive the equations describing current densities/potential gradients in the moving normal region, and to show how these equations may be resolved numerically. The temperature distribution may then be obtained without further difficulty (see Appendix).

3. Derivation of Equations

Examination of Fig. 4 shows that at reasonably low velocities the current will enter and leave the superconducting phase exclusively across the interphase boundary. For this reason it is only necessary to analyze the region *a–d* in Fig. 5, and as the normal phase can be considered as any other good conductor, only one set of equations is required. From Maxwell's equations, neglecting displacement currents.

$$\nabla \times \nabla \times \bar{E} = -\mu\sigma(\partial \bar{E}/\partial t), \tag{1}$$

from where we obtain the pair of coupled equations in two dimensions:

$$(\delta^2 E_y/\delta X\, \delta Y) - (\delta^2 E_x/\delta Y^2) = -\mu\sigma(\delta E_x/\delta t), \tag{2a}$$

$$(\partial^2 E_x/\partial X\, \partial Y) - (\partial^2 E_y/\partial X^2) = -\mu\sigma(\partial E_x/\partial t). \tag{2b}$$

The change of variable $\xi = X - vt$, where v is displacement velocity and t is time, leads to

$$-(\partial^2 E_y/\partial \xi\, \partial Y) + (\partial^2 E_x/\partial Y^2) = -\mu\sigma v(\partial E_x/\partial \xi), \tag{3a}$$

$$-(\partial^2 E_x/\partial \xi\, \partial Y) + (\partial^2 E_y/\partial \xi^2) = -\mu\sigma v(\partial E_y/\partial \xi), \tag{3b}$$

and further manipulation yields

$$(\partial^2 E_x/\partial \xi^2) + (\partial^2 E_x/\partial Y^2) = -\mu\sigma v(\partial E_x/\partial \xi), \tag{4a}$$

$$(\partial^2 E_y/\partial \xi^2) + (\partial^2 E_y/\partial Y^2) = -\mu\sigma v(\partial E_y/\partial \xi), \tag{4b}$$

and the continuity equation

$$(\partial E_x/\partial \xi) + (\partial E_y/\partial Y) = 0. \tag{5}$$

Either Eq. (4a) or (4b) (one is redundant) in conjunction with Eq. (5) can be used to describe the current distribution in the region of interest. Equations (3a) and (3b) are unsuitable for computational purposes due to the cross differential terms.

4. Boundary Conditions

The boundary conditions are complex and in some respects difficult to define. A major problem arises from the nature of the normal/superconducting interphase boundaries. In principle, these boundaries are defined by the critical temperatures T_c of the material as a function of local current density and, due to coherence effects, will be a region of change rather than an abrupt demarcation line. Though

in very thin films it is reasonable to assume a uniform current density in the superconducting phase, in thicker films a true current distribution would have to be computed. Furthermore, there is no reason to believe that the temperature will be uniform on a film cross section normal to the direction of motion, so even for very thin films it is unlikely that the interphase boundary will be normal to the direction of motion.

To resolve this problem it is necessary to use an iterative approach, correcting assumed initial boundary geometries on the basis of calculated temperatures and current distributions, repeating the process until no further corrections are required. Apart from possible convergence problems the computational effort required is excessive, and due to the coherence length effects the results would be inaccurate.

To avoid the complexities of the above procedure the author has preferred to work with a simple boundary geometry, normal to the direction of motion, and with uniform current density in the superconducting phase (constant T_c). The total current or the He bath temperature may then be adjusted until the calculated temperatures approximate T_c at the boundaries. Though the results obtained will be inaccurate, the errors will not be too large, and a useful guide to the magnitudes and distributions of the temperatures in the composite film will be obtained. The region of calculation is then limited to the rectangle AC FD (Fig. 5) in which AB and DE represent the interphase boundaries, over which $J_x = ct$, $J_y = 0$.

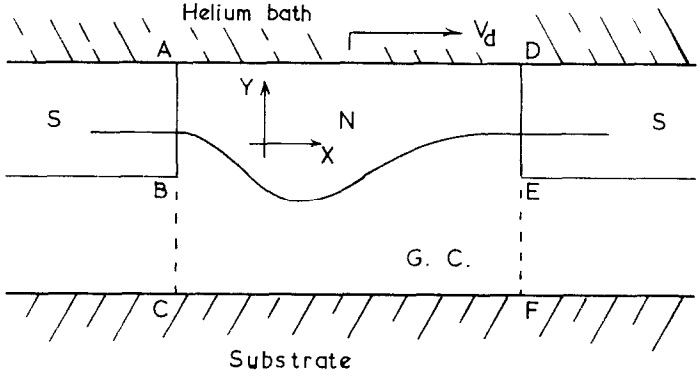

FIG. 5. Boundaries for computational purposes.

Over BC and EF, $J = 0$, hence $J_x = J_y = 0$ and the remaining problems concern AD and CF. Let us consider a series of superimposed films, alternating superconductor/good conductor, as in Fig. 6. The thicknesses of films of the same type are all equal. Then, if all the superconducting films carry equal biasing currents, and have identical normal regions, the current distribution shown in Fig. 6 is expected.

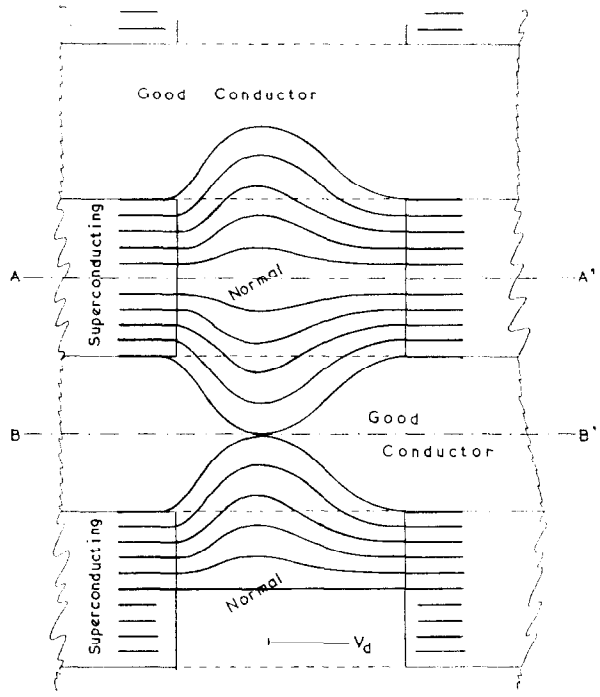

FIG. 6. Mirror image symmetries used for establishing boundary conditions.

If the films are now cut and separated along the symmetry planes A–A′ and B–B′ the current patterns will remain unaltered. Replacing the region above A–A′ and below B–B′ by nonmagnetic insulators (He bath, substrate) will not alter the current patterns. Hence we deduce that for AD and CF (Fig. 5) the Neumann condition $\partial J/\partial Y = 0$ ($\partial J_x/\partial Y = \partial J_y/\partial Y = 0$) and the Dirichlet condition $J_y = 0$ apply. The former is equivalent to saying that at corresponding nodes m and $-m$ on opposite sides of the symmetry planes we have $J_{x_m} = J_{x_{-m}}$ and $J_{y_m} = -J_{y_{-m}}$. Thus, the discretized form of Eq. (4a) may be applied to the boundary nodes with only minor modifications.

5. COMPUTATIONAL ANALYSIS

It was mentioned in Section 3 that either Eq. (4a) or Eq. (4b) must be discarded as redundant. In some situations there may be little reason to choose one or the other, but for the present problem it is necessary to discard (4b) because it does not possess a unique solution ($E_{y_{i,j}} = 0$ is an obvious solution). Furthermore,

the solution of the continuity equation requires initial values along either AD or CF and must, therefore, be applied to E_y. For these reasons we will discuss (a) Eq. (4a) and (b) the continuity equation.

(a) *Equation* (4a). Though it is possible to obtain general analytical solutions to Eq. (4), the introduction of boundary conditions greatly complicates the analysis for all except the most idealized conditions. Hence, for any realistic geometry it is necessary to turn to numerical methods. These calculate the value of the dependent variable (E) at N points (nodes) distributed throughout the region of interest. The discretization process establishes one equation per node, so the numerical method reduces to the solution of N simultaneous equations, and the choice of method is dependent on the value of N.

In the present situation we are looking for small asymmetries in an essentially symmetrical current distribution, so it is the author's opinion that the separation between (uniformly distributed) adjacent nodes should be a small proportion ($< 5\%$) of the corresponding axial dimension of the region. If n is the number of rows and of columns, $N = n^2$ and direct methods require the storage of an $N \times N$ matrix (n^4 store locations if nonsymmetrical). For $n = 20$, at least 160 000 locations are required, the number rising rapidly as greater resolution is called for. For this reason iterative methods are to be preferred, provided convergence can be established, even though the reduced storage ($\approx n^2$) is achieved at the expense of running time.

A convenient iterative scheme is successive over relaxation (SOR) applied to the Gauss–Seidel method (block iterative relaxation methods would theoretically yield improved convergence rates, but it seems doubtful whether the improvements would compensate for extra time involved in solution of implicit equations). It can be shown that the Gauss–Seidel method will converge when the matrix of the discretized equation has diagonal dominance and is irreducible. Considering Eq. (4a), its discretized form yields

$$E_{x_{i,j}} = [h^2k^2/2(h^2 + k^2)][(E_{x_{i+1,j}} + E_{x_{i-1,j}})(1/h^2) + (E_{x_{i,j+1}} + E_{x_{i,j-1}})(1/k^2) + (\mu\sigma v/2h)(E_{x_{i+1,j}} - E_{x_{i-1,j}})], \tag{6}$$

where $E_{p,q}$ is the value of E_x at the node in column p, row q, and h, k are spacings between columns and rows, respectively.

Examination of the matrix reveals that the condition for diagonal dominance,

$$\sum_{\substack{J=1 \\ J \neq i}}^{n} [E_{i,j}] \leqslant [E_{i,i}] \tag{7}$$

with strict inequality for at least one value of i, can be guaranteed by the inequality

$$\mu\sigma vh < 2, \tag{8}$$

while the method of directed graphs can be used to show that it is irreducible.

(b) *The continuity equation.* The solution to (4a) yields, subject to appropriate boundary conditions, the value of E_x at each node. The value of E_y must then be obtained using Eq. (5). An immediate problem is that the discretized form of this equation does not yield an explicit value of $E_{y_{i,j}}$. We can however, use the Taylor expansion

$$f(x) = f(a) + f^{i}(a)(X - a) + f^{ii}(a)(X - a)^2/2! + \cdots + f^{n}(a)(X - a)^n/n!, \tag{9}$$

the values of $f^n(a)$ being computed from Eq. (5) as follows:

$$f^{i}(a) = \partial E_y/\partial Y = -\partial E_x/\partial X, \tag{10}$$

$$f^{ii}(a) = \partial^2 E_y/\partial Y^2 = -\partial^2 E_x/\partial X\,\partial Y = \partial f^{i}(a)/\partial Y, \tag{11}$$

$$f^{n}(a) = \partial^n E_y/\partial Y^n = -\partial^n E_x/\partial X\,\partial Y^{n-1} = \partial^{n-1} f^{i}(a)/\partial Y^{n-1}. \tag{12}$$

These differential terms may be expanded in terms of central differences as follows:

$$f^{i}(a_0) = (1/h)[\delta_0{}^1 - (\delta_0{}^3/6) + (\delta_0{}^5/30) - (\delta_0{}^7/140) + \cdots], \tag{13}$$

$$f^{ii}(a_0) = (1/h^2)[\delta^2{}_0 - (\delta_0{}^4/12) + (\delta_0{}^6/90) - \cdots], \tag{14}$$

$$f^{iii}(a_0) = (1/h^3)[\delta_0{}^3 - (\delta_0{}^5/4) + \cdots], \tag{15}$$

$$f^{iv}(a_0) = (1/h^4)[\delta_0{}^4 - (\delta_0{}^6/6) + \cdots], \tag{16}$$

in which $\delta_0{}^n$ is the n-th order central difference term, corresponding to a_0 [19, p. 51].

The program outline is then fairly simple: The central difference terms for E_x are tabulated for each node, Eq. (13) being then used to compute $\partial E_x/\partial X$ at all nodes. It is then possible to tabulate central difference terms for $\partial E_y/\partial Y$ $(= -\partial E_x/\partial X)$ at all nodes, from which higher order derivatives may be calculated using Eqs. (13)–(16). Equation (9) and the boundary values for $E_{y_{i,0}}$ yield $E_{y_{i,1}}$. Repetition yields $E_{i,j}$ for $1 < j \leqslant n$, the last value being used as a check on overall accuracy as it must agree with the known boundary conditions on row n.

6. Results

(a) *Convergence of the SOR Program*

A computer program was written embodying the preceding conclusions. The determination of acceleration factors followed the scheme outlined by Carré [18].

TABLE I

Error Estimates [18] after Each 12 Cycle Group.[a]

cycles \ $\mu\sigma vh$	$0.6\pi = 1.884$ $v\ 0.3 \times 10^6$ m/sec	$0.68\pi = 2.13$ 0.34×10^6 m/sec	π 0.5×10^6 m/sec	$1.4\pi = 4.396$ 0.7×10^6 m/sec	2π 1.0×10^6 m/sec	0.041 5.4×10^6 m/sec
	V/m	V/m	V/m	V/m	V/m	V/m
2–13	7.68×10^{-3}	1.34×10^{0}	-1.20×10^{2}	-6.76×10^{7}	-1.59×10^{19}	1.98×10^{1}
14–25	2.43×10^{-4}	5.39×10^{0}	-2.89×10^{2}	-2.00×10^{6}	-4.28×10^{17}	6.31×10^{-1}
26–37	-1.43×10^{-6}	-7.88×10^{-2}	-3.82×10^{-1}	2.45×10^{2}	-7.98×10^{18}	-2.73×10^{-1}
38–49	-2.89×10^{-8}	-2.72×10^{-1}	-8.85×10^{-4}	-3.02×10^{10}	-2.60×10^{17}	-2.75×10^{-1}
50–61	1.01×10^{-8}	-3.50×10^{-2}	8.50×10^{-10}	6.85×10^{8}	-6.78×10^{17}	-6.39×10^{-1}
62–73	-3.21×10^{-8}	6.52×10^{-4}	5.78×10^{-10}	-5.05×10^{5}	-2.60×10^{18}	9.80×10^{-1}
74–85	-5.23×10^{-8}	3.71×10^{-5}	7.36×10^{-10}	-8.15×10^{2}	-1.71×10^{17}	1.25×10^{0}
86–97	5.43×10^{-10}	-5.89×10^{-12}	2.90×10^{-11}	-1.09×10^{4}	-7.46×10^{18}	2.15×10^{-1}
98–109	1.81×10^{-18}	-3.98×10^{-13}	-7.69×10^{-11}	-6.20×10^{5}	-2.74×10^{18}	1.30×10^{-1}
110–121	-4.19×10^{-15}	-1.56×10^{-21}	-6.68×10^{-13}	2.62×10^{3}	3.36×10^{17}	-6.66×10^{-3}
122–133	1.02×10^{-18}	1.07×10^{-18}	1.91×10^{-18}	-2.17×10^{2}	8.72×10^{16}	6.25×10^{-4}
134–145	0.00×10^{-99}	5.93×10^{-21}	4.60×10^{-22}	-6.23×10^{-3}	1.474×10^{14}	1.41×10^{-5}

[a] Interphase Boundary values: $E_x = 176$ V/m. Initial values: $E_x = 88$ V/m.

A 37 × 37 mesh was used ($n^4 \approx 1.8 \times 10^6$), providing reasonable resolution and the facility for intermediate abridged (10 × 10) printouts every 12 iterations. Convergence tests were performed using the following parameters:

$$h = k = 5 \times 10^{-8}\ m,$$

$$\mu = 4\pi \times 10^{-7}\ H/m,$$

$\sigma = 10^8\ (\Omega - m)^{-1}$ (assumed equal for good conductor and normal phase).

For $\mu\sigma vh = 2$, $v = 10^6/\pi = 0.318 \times 10^6$ m/sec. The program was tested for $\mu\sigma vh = 1.885$, 2.136, π, 4.396 and 2π. Table I shows the behavior of the error estimates [18], while the calculated values of acceleration factor are shown in Fig. 7. It can be seen that for $\mu\sigma vh \leqslant \pi$ the error estimates are small and reducing, even though the acceleration factors B [ratio (actual/calculated) nodal increments]

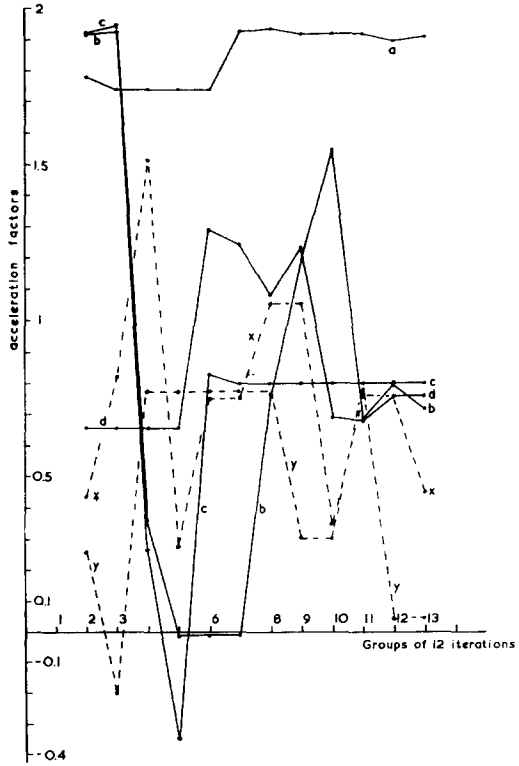

FIG. 7. Acceleration factors used in SOR programs, calculated according to Carré [18]; convergent for $\mu\sigma vh = 0.041$ (a), 1.884 (b), 2.13 (c) and π (d); nonconvergent for $\mu\sigma vh = 4.396$ (x) and 2π (y).

are generally greater than 0.7. The largest errors in this group occur for B close to 1.9 ($\mu\sigma v\, h = 0.041$). For $\mu\sigma v\, h > \pi$ the errors do not appear to follow any regular pattern and are large even though B is generally below 0.7. The single low value in this group (last value for $\mu\sigma v\, h = 1.4\pi$) occurs for $B < 0.05$ and may well be coincidental, but the author has not performed further iterations to check this point. It is clear that convergence is obtained for $\mu\sigma v\, h \leqslant \pi$; so not only does the SOR method converge when the matrix is diagonally dominant, but it will also converge when the off-diagonal terms are slightly dominant.

(b) *Accuracy*

The error estimates of Table I give an indication of the accuracy with which the iterative solution approaches the true solution to the difference equations. To estimate the corresponding accuracy for the E_y solution we may use two methods:

(i) The program for the continuity equation does not use the lower boundary values for E_y. Hence, it is possible to calculate these values using the results of the E_x iterations and the remaining boundary conditions. A comparison between calculated and known values will give a useful indication of magnitudes of errors.

(ii) The net current across any row must total zero. Hence, the algebraic sum of the values of E_y on any row must also be zero. The error, as a percentage of the sum of $|E_y|$ at all nodes on the row, will again be an indication of the accuracy of the solution. A typical calculation on a 37×37 mesh, using the parameters:

$$\left.\begin{aligned} h &= k = 11.25 \times 10^{-8}\ \text{m},\\ \mu &= 4\pi \times 10^{-7}\text{H/m},\\ \sigma &= 5.36 \times 10^{6}(\Omega - \text{m})^{-1},\\ v &= 5.4 = 10^{6}\text{m/sec}, \end{aligned}\right\} \qquad \mu\sigma v h = 0.041,$$

was run with $E_x = 176$ V/m at interphase boundaries and $E_x = 88$ V/m as initial condition at internal nodes. Acceleration factors and error estimates are shown in Fig. 7 and Table I. The following results were noted:

$$E_{x_{i,j}}(\min) = 2.88\text{V/m},$$

$$E_{y_{i,j}}(\min) = E_{y_{17,36}} = 5.92 \times 10^{-3}\text{V/m},$$

$$E_{y_{i,37}}(\max) = E_{y_{2,37}} = 3.12 \times 10^{-2}\text{V/m}.$$

$$\text{(i)}\ E_{y_{i,37}}/E_{y_{i,j}} \leqslant 0.1, \qquad \begin{matrix} 2 \leqslant j \leqslant 36 \\ 2 \leqslant i \leqslant 36, \end{matrix}$$

$$\text{(ii)}\ \sum_{i=1}^{37} E_{y_{i,j}} < 0.01 \sum_{i=1}^{37} |E_{y_{i,j}}|, \qquad 2 \leqslant j \leqslant 36.$$

(c) *Asymmetry*

Figures 8 and 9 show, respectively, the effects of velocities of 5.4×10^6 and 5.4×10^7 m/sec on a 400×10^{-10} m overall thickness film. The normal region is taken to be 400×10^{-10} m long, while $\mu = 4\pi \times 10^7$ H/m and $\sigma = 5.36 \times 10^6$ m/sec. The magnitude and direction of current density at each

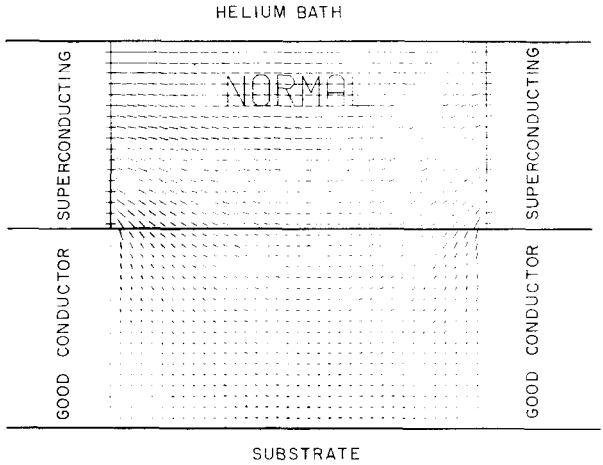

FIG. 8. Computed current flow patterns in normal region and adjacent conductor for a composite film thickness of 400×10^{-10} m, normal region length $l = 400 \times 10^{-10}$ m, and $\mu\sigma vh = 36.5 \times 10^{-6}$ m^{-1}. The magnitude and direction of current flow at each node is represented by the magnitude and direction of a line centred on the node. Direction of motion is to the left.

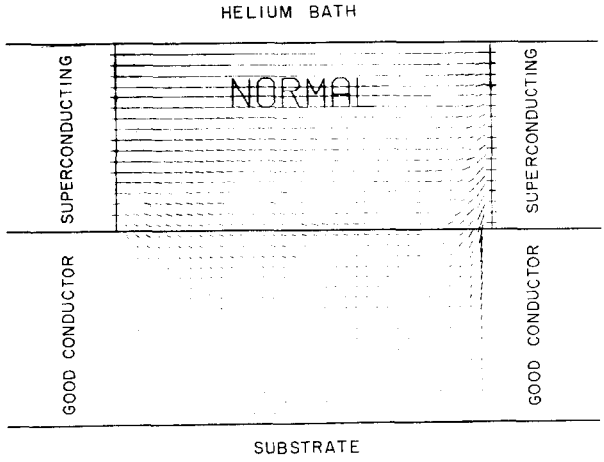

FIG. 9. As Fig. 8, but with $\mu\sigma vh = 36.5 \times 10^{-5}$ m^{-1}.

node on a 37 × 37 mesh is represented by the magnitude and direction of a line centered on the node. Figure 8 shows that $\mu\sigma v \approx 40 \times 10^{-6}$ m^{-1} is sufficient to produce discernible asymmetry in films of this thickness.

APPENDIX: Temperature Distribution

Though the solution to the temperature problem is, in mathematical terms, quite simple, it is also, for presently available materials, a very large computational problem. The reasons for this difficulty are discussed elsewhere [16, 20] but may be summarized as follows:

The thermal conductivities λ of presently available materials (say Sn, Cu) are of the order of 2000 W/(m − K) [21], while the coefficient for heat transfer α between the thin films and the substrate (taken to be an infinite heat sink) is of the order of 1000 W/(m^2 − K) [22]. The coefficient for direct transfer to the He bath is much lower and may be neglected [22]. Simple analysis then yields

$$(T - T_{\mathrm{He}}) = (T_c - T_{\mathrm{He}}) \exp[(-\alpha/\lambda t)^{1/2}\, l]$$

for the temperature T in a composite film of thickness t, at a distance l away from the interphase boundaries. Hence T will tend to T_{He} only when $l \gg t$. For this situation a two dimensional numerical solution is impractical due to the overall dimension of the region of analysis. Furthermore, this situation is unsuitable for satisfactory line operation, which must wait for more suitable materials [20].

The mathematical problem has been resolved as follows: The general equation for the temperature rise θ $(= T - T_{\mathrm{He}})$ is

$$\nabla^2\theta - (C\gamma/\lambda)(\partial\theta/\partial t) + G[X, Y, Z] = 0, \tag{17}$$

where $G[X, Y, Z]$ represents the effects of heat generation, C = heat capacity and γ = density. At the surfaces the rate of heat exchange is

$$dg/dt = \alpha \cdot \Delta\theta,$$

and must equal the rate of heat flow normal to the surface:

$$\alpha \cdot \Delta\theta = \lambda(d\theta/dN). \tag{18}$$

As before, we use $\xi = X - vt$ and rewrite Eq. (17) in two dimensions, as

$$(\partial^2\theta/\partial\xi^2) + (\partial^2\theta/\partial Y^2) - (c\gamma v/\lambda)(\partial\theta/\partial\xi) + W(\xi, Y) = 0, \tag{19}$$

where

$$W[\xi, Y] = J_{i,j}^2\, \rho. \tag{20}$$

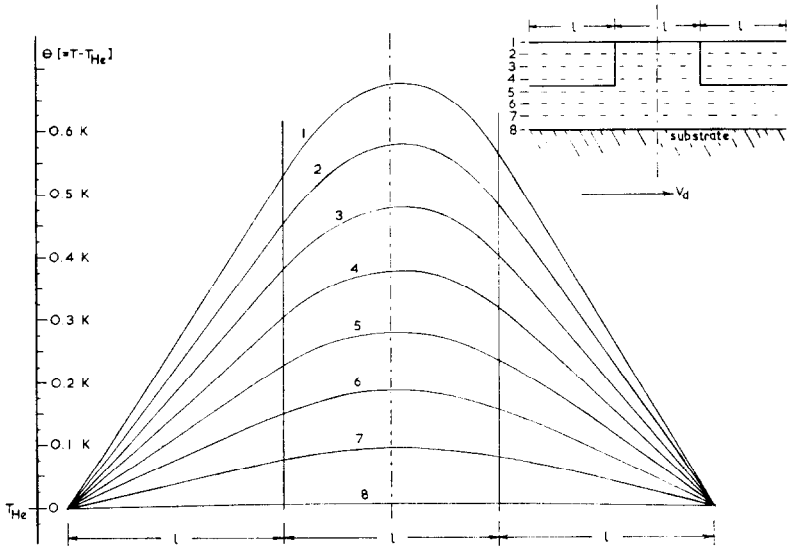

FIG. 10. Calculated temperature distributions in a moving normal region and the adjacent good conductor and superconducting phase. The temperature curves 1–8 correspond to the lines 1–8 on the inset diagram.

Equation (19) is similar to Eq. (4a) and may be resolved in the same manner. A program has been written, and typical results are shown in Fig. 10. The assumed conditions were:

overall film thickness $t = 3140 \times 10^{-10}$ m,

normal region length $l = 3140 \times 10^{-10}$ m,

$\mu = 4\pi \times 10^{-7}$ H/m,

$\sigma = 10^{8}(\Omega - \text{m})^{-1}$,

$v = 3 \times 10^{5}$ m/s,

$h = 112.5 \times 10^{-10}$ m,

$(\mu\sigma vh) = 0.425$,

$J = 1.76 \times 10^{12}$ A/m^2,

$\lambda = 2000$ W/(m $-$ K),

$\alpha = 1000$ W/(m^2 $-$ K).

θ is assumed to have fallen to zero at a distance l from the interphase boundaries, in order to reduce the size of the problem. Even so, the mesh contains 1465 nodes (29×85) and the solution is available after 240 temperature iterations. Examina-

tion of Fig. 10 reveals two points: (a) the temperature rise is nonsymmetrical, and (b) the assumed interphase boundaries require modification until they agree with computed results [16]. The nonsymmetries are less pronounced than those which would be obtained with reduced λ.

REFERENCES

1. H. D. CRANE, Technical Report No. 1506-2, AD240306, Stanford University, Stanford, CA, 1960.
2. H. D. CRANE, *IRE Trans. Elect. Comp.* **EC-9** (1960), 370–371.
3. H. D. CRANE, Interim Report 1, Project 3286, AD250305, Stanford Research Institute, Stanford, CA, 1960.
4. H. D. CRANE AND A. ROSENGREEN, Interim Report 2, Project 3286, AD250826, Stanford Research Institute, Stanford, CA, 1960.
5. A. J. COTE, *Proc. IRE.* **49** (1961), 1430–1431.
6. A. C. SCOTT, *Proc. IEEE.* **51** (1963), 240.
7. J. NAGURNO, S. ARIMOTO AND S. YOSHIZAWA, *Proc. IRE.* **50** (1962), 2061–2070.
8. A. J. COTE, *Electronics* **34** (1961), 51–53.
9. S. RAZI, Project 1510-31, Electronics Laboratory, Stanford University, CA, 1960.
10. H. KUNOV, *Electron. Lett.* **1** (1965), 134.
11. A. ROSENGREEN, *Electronics* **36** (1963), 25–27.
12. R. D. PARMENTIER, *Solid State Electron.* **12** (1969), 287–297.
13. D. R. CHAMBERS, Interim Report 8, Project 3286, AD607199, Stanford Research Institute, Stanford, CA, 1964.
14. F. A. PADOVANI, Quarterly Status Report 10, pp. 18-23, Solid State Electronics Research, Stanford University, Stanford, CA.
15. R. F. BROOM AND E. H. RHODERICK, *Brit. J. Appl. Phys.* **11** (1960), 292–296.
16. D. C. BARKER, Ph.D. thesis, University of Manchester Institute of Science and Technology, Manchester, U.K., 1970.
17. R. S. VARGA, "Matrix Iterative Analysis," Prentice-Hall, Englewood, Cliffs, NJ, 1962.
18. B. A. CARRÉ, *Comput. J.* **4**, 73–78.
19. R. A. BUCKINGHAM, "Numerical Methods," Pitman, 1962.
20. D. C. BARKER, The feasibility of a proposed superconducting neuristor realization. *IEEE Trans. Electron. Devices*, ED-19 (1972).
21. National Bureau of Standards, "Properties of Materials at Low Temperatures—A Compendium" WADD Tech. Report 60-56.
22. H. SEKI AND I. AMES, *J. Appl. Phys.* **38** (1964), 2069–73.
23. M. W. GREEN, "Cryogenic Neuristor Employing Induction Means to Control Superconductivity," U.S. Patent Office, No. 3 218 482, 1965.